Axion-mediated Transport of Fast Radio Bursts Originating in Inner Magnetospheres of Magnetars

Anirudh Prabhu [ORCID]
Princeton Center for Theoretical Science, Princeton University, Princeton, NJ 08544, USA
Received 2023 February 28; revised 2023 March 23; accepted 2023 March 26; published 2023 April 6

Abstract

Among magnetar models of fast radio bursts (FRBs), there is ongoing debate about whether the site of coherent radio emission lies within or beyond the light cylinder. We propose a mechanism by which FRBs produced near the magnetar surface are transported out of the magnetosphere by axions, which are hypothetical particles that couple to photons. If the emission site hosts strong accelerating electric fields, a considerable fraction of the FRB energy budget is converted to an axion burst. Once produced, the axion burst free streams out of the magnetosphere due to the rapidly decreasing magnetic field. The burst may escape through either the open or closed magnetosphere while retaining the temporal signature of the original FRB. In the wind region, axions resonantly excite ordinary (O) modes that escape as the plasma density decreases. The radio efficiency of this mechanism satisfies energetics constraints from FRB 121102 for axion−photon coupling strengths that have not been excluded by other astrophysical probes.

Unified Astronomy Thesaurus concepts: Radio transient sources (2008); Magnetars (992); Particle astrophysics (96); Cold dark matter (265); Radio pulsars (1353); Rotation powered pulsars (1408); Plasma astrophysics (1261)

1. Introduction

Fast radio bursts (FRBs) are ultraluminous, millisecond-duration radio transients that are usually of extragalactic origin. Their short durations, with pulse substructure at the microsecond scale, are suggestive of a compact object central engine, such as a neutron star or stellar mass black hole (Katz 2017; Li et al. 2018; Katz 2020; Sridhar et al. 2021; Katz 2022). Recent detection of an FRB associated with galactic magnetar SGR 1935+2154 provides support for the claim that at least a subset of FRBs are sourced by magnetars. The high brightness temperature (in excess of 10^{30} K) necessitates a coherent emission mechanism. Within magnetar models there are two broad categories for the emission: magnetospheric models, in which the radio waves are produced within the light cylinder ($r \ll R_{\rm LC} \equiv c/\Omega$, where Ω is the rotational frequency of the magnetar), and far-field models, in which the radio waves are produced outside the light cylinder, possibly in the wind or nebula regions. Examples of magnetospheric models include coherent radiation by charged bunches (Ruderman & Sutherland 1975; Kumar et al. 2017; Kumar & Bošnjak 2020; Lu et al. 2020) and inner-magnetosphere reconnection (Lyubarsky 2020).[1] Far-field models often rely on magnetosphere ejecta sourced by magnetar flares forming blast waves in the wind that emit coherent radio waves through the synchrotron maser process (Beloborodov 2017; Metzger et al. 2019; Beloborodov 2020) or reconnect with magnetic fields outside the light cylinder, leading to radio emission through the collision of small magnetic plasmoids (Philippov et al. 2019; Lyubarsky 2020; Yuan et al. 2020; Mahlmann et al. 2022).

---

[1] The author posits that inner-magnetosphere reconnection necessarily takes place, but any FRB produced therein cannot escape.

Arguments in favor of magnetospheric models are that they are able to explain the rapid variability of FRB pulses, down to 60 ns from FRB 20200120E (Nimmo et al. 2022), the rapid polarization swings observed in some FRB pulses (Luo et al. 2020), and the relatively high expected radio efficiency of inner-magnetosphere mechanisms. One issue that inner-magnetosphere models must contend with is how an FRB produced in the inner magnetosphere can escape. As an FRB produced in the inner magnetosphere propagates through the lower-density outskirts of the magnetosphere, it strongly scatters with the plasma and loses much of its energy to acceleration of charged particles (Beloborodov 2021). Models invoking coherent emission by charged bunches circumvent these issues by resorting to emission along open field lines, where radio photons may easily escape (Kumar et al. 2017; Kumar & Bošnjak 2020; Lu et al. 2020). Highly beamed emission may be in tension with the high expected event rate of $\sim 10^4$ per day (Thornton et al. 2013). Far-field models struggle to explain rapid variability and polarization angle swings but can successfully explain the escape of radio waves since the FRB energy is transported out of the magnetosphere by magnetic flare ejecta and does not rely on beamed emission.

In this Letter, we propose a generic class of models in which FRBs produced in the inner magnetosphere are transported out of the magnetosphere by axions. Axions, broadly defined, are ultralight spin-0 bosons that arise in many extensions of the Standard Model (SM) of particle physics. The QCD axion was originally proposed to explain the seemingly unnatural smallness of the neutron electric dipole moment: a puzzle known as the "strong charge parity (CP) problem" (Peccei & Quinn 1977a, 1977b; Weinberg 1978; Wilczek 1978). The solution involves adding to the SM a new symmetry, called the Peccei–Quinn (PQ) symmetry, which is spontaneously broken, and a new particle, the QCD axion, which is charged under PQ symmetry. In the simplest QCD axion models, the scale of PQ symmetry breaking determines the axion mass and coupling strength to SM fields up to $\mathcal{O}(1)$ model-dependent factors.

Axion-like particles (ALPs) are a generalization of the QCD axion and arise generically in many extensions of the SM including string theory (Svrcek & Witten 2006; Arvanitaki et al. 2010). Though they share many properties of the QCD axion, ALPs do not necessarily address the strong CP problem. Various string theories predict the existence of a plenitude of ALPs with a wide range of masses and coupling strengths to SM fields (Mehta et al. 2021). Thus, in astrophysical and laboratory probes of ALPs, the mass and coupling strengths are treated as independent, free parameters.

We comment that QCD axions and ALPs are produced nonthermally in the early universe and are among the best-motivated candidates to account for the ≈85% of matter density in the universe that exists in the form of some cold dark matter (Sikivie 1983; Dine & Fischler 1983; Preskill et al. 1983). The models proposed in this Letter are agnostic to the relationship between axions and dark matter and thus apply as long as axions exist in nature. In the following discussion, we use the term "axion" to refer to both QCD axions and ALPs, drawing the distinction only when necessary.

Axions couple to electromagnetism through the two-photon interaction term,

$$\mathcal{L}_a = -g_{a\gamma\gamma} a(x) \mathbf{E} \cdot \mathbf{B}, \qquad (1)$$

where $a(x)$ is the axion field, $g_{a\gamma\gamma}$ is a coupling constant, and $\mathbf{E}$ and $\mathbf{B}$ are electric and magnetic fields. This coupling has been exploited in numerous astrophysical and laboratory searches for axions. There is extensive literature on the role of axions in high-energy astrophysical settings, such as in SN1987A (Burrows et al. 1990; Keil et al. 1997; Caputo et al. 2022; Hoof & Schulz 2022). Some constraints from SN1987A come from the fact that axions may efficiently transport energy from the supernova or remnant neutron star, leading to an additional cooling mechanism, analogous to neutrino cooling (Burrows et al. 1990). Extreme, highly magnetized plasmas also provide a good laboratory for axion searches. Large magnetic fields, such as those near the surfaces of pulsars and magnetars, greatly enhance the conversion rate between axions and photons. The effects of conversion of axion dark matter in neutron star magnetospheres have been explored (e.g., Pshirkov & Popov 2009; Huang et al. 2018; Hook et al. 2018; Safdi et al. 2019; Battye et al. 2020; Leroy et al. 2020; Foster et al. 2020; Buckley et al. 2021; Witte et al. 2021; Battye et al. 2021b, 2021a; Millar et al. 2021; Foster et al. 2022). Additionally, there are claims that collisions of axion stars with neutron stars might be the source of FRBs (Tkachev 2015; Iwazaki 2015; Pshirkov 2017; Prabhu & Rapidis 2020; Buckley et al. 2021). We emphasize that these proposals assume axions to be dark matter, which is not a requirement of our model.

In our model (see Figure 1 for a summary), an FRB produced near the surface of a magnetar efficiently converts to axions due to the strong magnetic field therein. Crucially, the axion burst retains the temporal structure of the FRB. As the axion burst propagates through the magnetosphere, its conversion rate back to photons becomes highly suppressed as the magnetic field decreases as $B_{\mathrm{dipole}} \propto r^{-3}$, allowing the burst to effectively free stream out of the magnetosphere. Once in the wind region, the axion burst experiences a plasma with decreasing plasma frequency. At a critical radius $r_c \gg R_{\mathrm{LC}}$
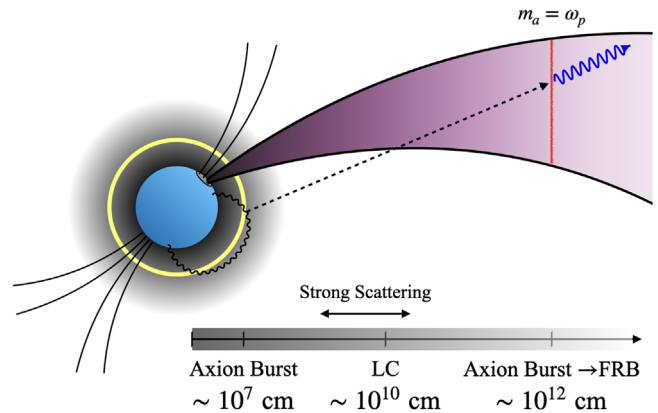

Figure 1. Summary of proposed mechanism. Axions (black dashed line) produced at a critical radius in the inner magnetosphere (yellow circle) propagate through the light cylinder (LC) to the dense, preflare wind (purple) and resonantly convert to radio photons (blue wavy line with arrow), which may escape. Relevant length scales are shown at the bottom of the image for a magnetar with rotational period $P = 1$ s and axion mass $m_a = 10^{-10}$ eV. See Section 4 for details of these length scales. The region where an FRB would scatter strongly with the plasma is labeled.

the plasma frequency coincides with the axion mass, $\omega_p(r_c) = m_a c^2/\hbar$, and the axion burst resonantly excites ordinary (O) waves that can escape the system. We show that in young magnetars, the radio efficiency of the proposed model is within energetics constraints from FRB 121102 for axion−photon couplings that satisfy high-energy astrophysical constraints. In this model, the FRB can escape through either the open or closed magnetosphere and thus does not rely on beaming.

The paper is organized as follows. In Section 2, we review the formalism of axion coupling to photons in a magnetized plasma, paying particular attention to regimes of strong coupling. In Section 3, we provide some general criteria for axion bursts to be produced in the inner magnetosphere. We relate this discussion to existing magnetospheric FRB models and argue that a large fraction of the FRB energy is converted to axions near the magnetar surface. Following their production, axions reconvert to outgoing radio photons in the enhanced preflare magnetar wind. We compute the efficiency of this reconversion in Section 4 and show the axion−photon coupling parameter space consistent with efficiency constraints in Section 5. We provide concluding remarks in Section 6.

2. Axion−Photon Mixing in Plasma

Axions interact with electromagnetism through the operator described by Equation (1). This interaction implies that axions can be generated electromagnetically in regions where $\mathbf{E} \cdot \mathbf{B} \neq 0$, such as in the vacuum gaps above pulsar polar caps (Prabhu 2021; Noordhuis et al. 2022). Equation (1) also leads to a nonlinear modification of Maxwell's equations that allows for interconversion between axions and photons.[2] By assuming 1D propagation in a magnetic field with a constant direction but gradually changing magnitude and by considering ultrarelativistic axions with energy (ω) much greater than their mass (m_a), the equation for axion−photon conversion in a plasma with

---

[2] For detailed treatments of nonrelativistic axion-to-photon conversion in magnetized, anisotropic plasmas, see Millar et al. (2021) and Witte et al. (2021). We emphasize that these studies consider nonrelativistic axion dark matter; thus, their results are not directly applicable to the case of relativistic axions presented in this work.

spatially varying frequency, $\omega_p(z)$, can be derived using the WKB approximation (see, e.g., Raffelt & Stodolsky 1988),

$$\left[i\partial_z + \omega \begin{pmatrix} 1 + \Delta_a & \Delta_{a\gamma} \\ \Delta_{a\gamma} & 1 + \Delta_{\parallel} \end{pmatrix} \right] \begin{pmatrix} a \\ A_{\parallel} \end{pmatrix} = 0, \qquad (2)$$

where a is the axion field and $A_{\parallel}$ is the photon state parallel to the background magnetic field and normal to the direction of motion (z-direction). The diagonal terms represent effective refractive indices with $\Delta_a = -m_a^2/(2\omega^2)$ and $\Delta_{\parallel} = -\omega_p^2/(2\omega^2)$. The refractive index receives a contribution from the Euler–Heisenberg term $\Delta_{\parallel,\mathrm{EH}} = (7\alpha/90\pi)(B/B_c)^2 \sin^2\theta$, where $B_c = m_e^2/e \approx 4.4 \times 10^{13}$ G is the Schwinger critical field (Raffelt & Stodolsky 1988; Fortin et al. 2021). We will discuss axion production at $\mathcal{O}(10)$ stellar radii, where $\Delta_{\parallel,\mathrm{EH}} \ll \omega_p^2/\omega^2 \sim 1$, so we neglect the Euler–Heisenberg term. The off-diagonal term, $\Delta_{a\gamma} = g_{a\gamma}B_0(z)\sin\theta/(2\omega)$, where $B_0(z)$ is the magnitude of the background magnetic field and θ is the angle between the magnetic field and the direction of propagation, quantifies the mixing between axion and photon states. Equation (2) resembles the Schrödinger equation, with z playing the role of time, and can be solved to first order in $\Delta_{a\gamma}$ using time-dependent perturbation theory, giving (Raffelt & Stodolsky 1988; Fortin & Sinha 2018, 2019; Dessert et al. 2019)

$$P = \left| \int_{z_i}^{z_f} dz' \omega \Delta_{a\gamma}(z') e^{i\Delta_a(z') - i \int_{z_0}^{z'} \Delta_{\parallel}(z'')dz''} \right|^2, \qquad (3)$$

where z_i and z_f are the initial and final locations, respectively. In general, the dispersion relations for the axion and photon are different, leading to dephasing over a propagation distance $\ell_d = 1/\Delta k$, where $\Delta k = |\sqrt{\omega^2 - \omega_p^2} - \sqrt{\omega^2 - m_a^2}|$ is the momentum mismatch between the two modes. If, however, the axion mass coincides with the plasma frequency, the mixing is resonantly enhanced. Axions propagating through a plasma with frequency $\omega_p(z) \propto z^{-n}$, where $n = 3/2$ corresponds to a Goldreich–Julian density profile and $n = 1$ corresponds to a spherically expanding wind, will resonantly convert at a critical distance, z_c where $\omega_p(z_c) = m_a c^2/\hbar$. Equation (3) can be solved in the stationary phase approximation to give

$$P_{\mathrm{res}} = \left(\frac{\pi}{n} \right) g_{a\gamma}^2 B(z_c)^2 \frac{\omega z_c}{\omega_p(z_c)^2}, \qquad (4)$$

where we have set $\hbar = c = 1$. The analysis above, applied to plane wave solutions, can be extended to generic wave packets. From Equation (4), we note that the conversion leads to spectral distortions, with more efficient conversion of higher frequency components. This is because at fixed axion mass, the momentum mismatch, $\Delta k \approx |\omega_p^2 - m_a^2|/2\omega$, is smaller for higher frequencies. We also note that the axion and photon wave packets experience dispersive spreading. Since in the resonant conversion region, the dispersion relations for axions and photons are roughly the same, this effect is indistinguishable from dispersion of an electromagnetic wave propagating through a plasma.

3. Axion Production in the Inner Magnetosphere

We outline some general criteria for an FRB produced in the inner magnetosphere to convert efficiently into axions. First, a strong electric field component parallel to the background magnetic field ($E_{\parallel}$) must be present in the emission region. Parallel electric fields arise generically in models of persistent and transient emission in compact objects. Dynamical screening of $E_{\parallel}$ by pair cascades, leading to the emission of superluminal O modes, is thought to be the mechanism behind pulsar radio emission from polar caps (Philippov et al. 2020; Ruderman & Sutherland 1975). A similar mechanism can take place due to crustal motion of magnetars with low magnetospheric twist, leading to FRBs emitted along closed field lines (Wadiasingh & Timokhin 2019; Wadiasingh et al. 2020). During a magnetar flare, magnetic reconnection is likely to take place in the inner magnetosphere (Lyubarsky 2020) and is generically expected to host $E_{\parallel}$ in three dimensions (Schindler et al. 1988). Another class of proposed inner-magnetosphere models involves the formation of charged bunches that emit coherent curvature radiation (Kumar & Bošnjak 2020; Lu et al. 2020). In this Letter, we study axion production within this model though we emphasize that the general mechanism of axion transport applies to any inner-magnetosphere emission mechanism that hosts large $E_{\parallel}$. We investigate axion production in near-surface magnetic reconnection in future work.

3.1. Axion Production by Charge-starved Alfvén Waves

In this section, we review the model of Kumar & Bošnjak (2020) and compute the efficiency of axion production in this model. The starting point of this model is the release of an enormous amount of magnetic energy during a magnetic flare. This disturbance to the magnetosphere launches Alfvén waves from close to the magnetar surface, which propagate along the dipole magnetic field lines. The waves require a current along the magnetic field lines, supported by counterpropagating $e^{\pm}$ pairs accelerated to very high Lorentz factors. The counterpropagating charges are susceptible to a two-stream instability that generates a large $E_{\parallel}$, and considerable flux of axions. Below, we provide the details of this model.

For simplicity, we describe the propagation of Alfvén waves in a constant magnetic field, $B_0\hat{z}$, which we will show is a good approximation for the system under consideration. The Alfvén wave can be described as a magnetic perturbation in the $\hat{y}$ direction that propagates in the $x - z$ plane, $\delta\boldsymbol{B} = B_y\hat{y}\exp[i(k_{\perp}x + k_{\parallel}z - \omega_A t)]$, where $B_y = \varepsilon B_0$ and $\varepsilon \ll 1$. For Alfvén waves, the perpendicular component of the wavevector decreases with distance from the magnetar surface as $r^{-3/2}$ (Lu et al. 2020). Thus $k_{\perp} \ll k_{\parallel}$ in general, confirming that a 1D treatment is a good approximation. The amplitude of the Alfvén wave also decays with radius due to propagation effects (Lu et al. 2020) and the development of the two-stream instability, but the former occurs over large length scales. We work in the approximation in which the two-stream instability and the axion field do not strongly modulate the Alfvén wave. This is supported by simulations in Kumar et al. (2022), which show that the maximum amplitude of $E_{\parallel}$ generated in the two-stream instability is $\sim 0.1 B_y$, and that treating the prespecified magnetic perturbation defined above to be fixed is a good approximation. At a distance of $\mathcal{O}(10)$ stellar radii, the Alfvén wave encounters an upstream medium with low number density. The evolution of $E_{\parallel}$ and the axion field are described by

Ampère's law and the Klein–Gordon equation,

$$\partial_t E_\parallel + j_\parallel^{(1)} - \partial_t \theta B_0 = (\boldsymbol{\nabla} \times \delta \boldsymbol{B})_z - j_\parallel^{(2)} \tag{5}$$

$$\partial_t^2 \theta - \nabla^2 \theta + m_a^2 \theta = -g_{a\gamma\gamma}^2 B_0 E_\parallel, \tag{6}$$

where $\theta(x) \equiv g_{a\gamma\gamma} a(x)$ is the dimensionless axion field. As in Kumar et al. (2022), we have split the current density into two parts: $j_\parallel^{(1)}$ is the current density of the upstream medium, and $j_\parallel^{(2)}$ is the current density advected by the Alfvén wave. Even in the absence of an upstream medium, a small Coulomb field is generated as the charged particles in the Alfvén wave lag behind the wave, leading to a contribution to the right hand side of Equation (5). The lag between the particles and the Alfvénwave grows with time, leading to (Kumar et al. 2022)

$$E_\parallel(z, t) = \frac{B_y(z, t) \omega_A t}{2\gamma_0^2} \left(\frac{k_\perp}{k_\parallel} \right), \tag{7}$$

where γ_0 is the Lorentz factor of particles advected by the Alfvén wave. For axions with mass $m_a \lesssim \omega_A$ the displacement current drives the axion field at frequency ω_A. Alfvén waves have a high reflection coefficient at the magnetar surface, allowing them to bounce along field lines in the magnetosphere many times (Li & Beloborodov 2015). This may lead to a prolonged, low-frequency axion counterpart at the Alfvén wave frequency. We investigate this effect in a future study.

3.2. Linear Stability Analysis: Two-stream Instability

Equations (5) and (6) may be unstable to small perturbations in $j_\parallel^{(2)}$. A detailed analysis of this two-stream instability was demonstrated analytically and numerically in Kumar et al. (2022). Small parameters, $E_\parallel$, θ, and $\delta j_\parallel^{(1)}$, are taken to have dependence $\propto \exp(ikz - i\omega t)$, where $k \in \mathbb{R}$ and $\omega \in \mathbb{C}$. Solutions to the perturbed equations with $\mathrm{Im}(\omega) \equiv \omega_i > 0$ correspond to exponentially growing solutions. The evolution of instabilities will be dominated by the fastest-growing modes, which have $\mathrm{Re}(\omega)$, $k \approx \omega_{p,1}$ and $\omega_i = \omega_{p,1}^{1/3} \omega_{p,2}^{2/3}/\gamma_0$, where $\omega_{p,1(2)} = \sqrt{e^2 n_{1(2)}/m_e}$. The subscript "1" corresponds to the upstream plasma and "2" to the plasma advected by the Alfvén wave (Kumar et al. 2022). From Equation (6), the conversion efficiency from $E_\parallel$ to axions is given by

$$\eta_{\gamma \to a} \equiv \frac{\omega^2 |a|^2}{|E_\parallel|^2} \simeq \frac{g_{a\gamma\gamma}^2 B_0^2 \omega_p^2}{(m_a^2 + \omega_i^2)^2 + 4\omega_p^2 \omega_i^2}$$

$$\approx 0.01 \times g_{10}^2 B_{0,13}^2 \omega_{i,-8}^{-2}, \tag{8}$$

where $g_{10} = g_{a\gamma\gamma}/(10^{-10}/\mathrm{GeV})$, $B_{0,13} = B_0/(10^{13}\,\mathrm{G})$, and $\omega_{i,-8} = \omega_i/(10^{-8}\,\mathrm{eV})$. The fiducial value of ω_i assumes $\omega_p = 2\pi$ GHz, $\varepsilon = 10^{-3}$, $k_\perp = 0.1\omega_A$, and $\gamma_0 = 1000$. The fiducial value of $g_{a\gamma\gamma}$ is approximately set to the bound from the CAST solar axion search (CAST 2017). In Equation (8), the conversion probability is independent of m_a only if $m_a \ll \omega_p$.

4. Reconversion in the Wind

Magnetars emit a persistent spin-powered wind with luminosity $L_w = \mu^2 \Omega^4 (1 + \sin^2 \alpha)$, where μ is the magnetic dipole moment of the magnetar, Ω its rotational frequency, and α the angle between the rotational and dipole axes (Li et al.
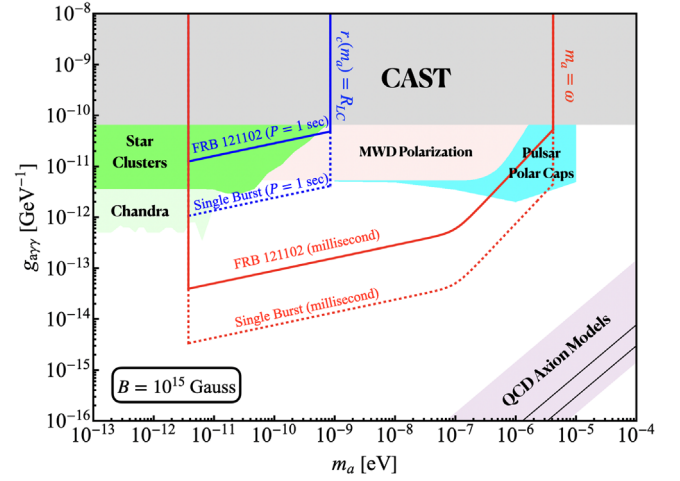

Figure 2. Minimum allowed axion–photon coupling consistent with efficiency constraints for a single burst (dashed) and from FRB 121102 (solid) assuming the source is a magnetar with surface field $B = 10^{15}$ G and rotational period $P = 1$ s (blue) or $P = 1$ ms (red). We assume a burst of fluence $F = 1\,\mathrm{Jy} \cdot \mathrm{ms}$ with central frequency $\nu = $ GHz and $\Delta\nu = \nu$. For the single burst, we have assumed a distance of $D = 1$ Gpc and conservatively set $z = 0$. For additional parameter values, see Section 5. We do not consider axion masses less than the plasma frequency of the ISM (see the end of Section 4). We set the fiducial value of the ISM plasma frequency to be that of the Milky Way. Parameter space excluded by other astrophysical probes is shaded (Wouters & Brun 2013; Marsh et al. 2017; Reynolds et al. 2020; Dessert et al. 2020; Sisk-Reynés et al. 2021; Dessert et al. 2022; Noordhuis et al. 2022). QCD axion models are shaded in light purple.

2012). The toroidal magnetic field in the wind is supported by a particle outflow, $\dot{N}$. Seconds before a magnetar flare, the wind luminosity and particle flow rates are greatly enhanced from their persistent values (Beloborodov 2017, 2020). The wind can be characterized by a magnetization σ_w and Lorentz factor Γ_w. At large distance, the wind Lorentz factor is approximately $\Gamma_w \sim 3 \times (L_w/\dot{N}m_e)^{1/3}$ (Beloborodov 2020). In general the wind is highly magnetized, giving $B_\phi^2(r) = L_w/(4\pi r^2)$ at large distance. The plasma frequency can be related to the particle flow rate as $\omega_p^2 = e^2 \dot{N}/(4\pi m_e r^2 \Gamma_w)$. The critical radius, r_c, at which axions resonantly convert to longitudinal O modes, and corresponding magnetic field strength are

$$r_c = 2 \times 10^{12}\,\mathrm{cm} \cdot L_{w,42}^{-1/6} \dot{N}_{40}^{2/3} m_{a,-10}^{-1}, \tag{9}$$

$$B_\phi(r_c) = 100\,\mathrm{G} \cdot L_{w,42}^{-2/3} \dot{N}_{40}^{-2/3} m_{a,-10}, \tag{10}$$

where $m_{a,-10} = m_a/(10^{-10}\,\mathrm{eV})$, $L_{w,42} = L_w/(10^{42}\,\mathrm{erg\,s^{-1}})$, and $\dot{N}_{40} = \dot{N}/(10^{40}\,\mathrm{s^{-1}})$. For reference, a young magnetar with surface field $B_s = 10^{15}$ G and rotation period $P = 0.1\,s$ would have persistent wind luminosity $L_{w,42} \approx 0.1$ and $\dot{N}_{40} = 10^{-4}\mathcal{M}$, where $\mathcal{M}$ is the multiplicity factor of pairs produced in the open field lines (Beloborodov 2020). Again, the preflare values of these parameters are expected to be much larger but are poorly constrained. In Figure 2 we adopt a fiducial enhancement factor of 10^2 for both L_w and $\dot{N}$ but emphasize that the results of this model are sensitive to these parameters and better estimates are required. From Equation (3), the resonant axion-to-photon conversion probability in the wind is

$$\eta_{a \to \gamma} \simeq 0.01 \times g_{10}^2 L_{w,42}^{7/6} \dot{N}_{40}^{-2/3} m_{a,-10}^{-1} \omega_{\mathrm{GHz}}, \tag{11}$$

where $\omega_{\mathrm{GHz}} = \omega/(2\pi\,\mathrm{GHz})$. We comment that at sufficiently low axion mass, resonant conversion takes place outside the

wind region, where Equation (11) does not apply. At a distance $r_{ts} \gg R_{LC}$ the wind collides with the surrounding medium and creates a "termination shock," which converts magnetic energy to particle kinetic energy (Kennel & Coroniti 1984; Slane 2017). Axion conversion is inefficient for $r > r_{ts}$ due to the absence of strong ordered magnetic fields therein. The asymptotic plasma frequency is equal to that of the interstellar medium (ISM), $\omega_{p,ISM}$. While the outer region of the wind has $\omega_p \ll \omega_{p,ISM}$, the discrepancy may lead to the development of Rayleigh–Taylor filaments (Porth et al. 2014) that strongly affect the conversion of axions into photons. To avoid these complications, we restrict our analysis to conversion radii $r_c \ll r_{ts}$ where $\omega_p(r_c) < \omega_{p,ISM}$, thus restricting $m_a < \omega_{p,ISM}$.

5. Efficiency Constraints

The energy reservoir for young magnetars comes from either the magnetic field ($E_{mag} \simeq 4\pi B_0^2 R_{ns}^3/3$) or rotation ($E_{rot} = M_{ns}R_{ns}^2\Omega_{rot}^2/5$). For the remainder of this section we take standard values for the neutron star mass ($M_{ns} = 1.4\,M_\odot$) and radius ($R_{ns} = 10\,\mathrm{km}$). The energy released in a single burst is

$$E = \frac{L_{iso}\tau}{\eta_r}\left(\frac{\delta\Omega}{4\pi}\right), \tag{12}$$

where L_{iso}, τ, η_r, and the term in the parentheses are the isotropic equivalent luminosity, duration, radio efficiency, and beaming factor of the burst, respectively. Upper limits on the radio energy of several FRBs were derived in Zhang (2018), giving $E\eta_r \sim 10^{40}$–10^{42} erg. The constraint that the total energy released in an FRB not exceed the available energy is

$$\eta_r \geqslant \frac{3\times 10^{-9}}{(1+z)}f_b\, D_{L,\mathrm{Gpc}}^2 F_{\nu,\mathrm{Jy\cdot ms}}\Delta\nu_{\mathrm{GHz}}B_{0,15}^{-2}, \tag{13}$$

where $D_{L,\mathrm{Gpc}}$ is the luminosity distance (in Gpc), $F_{\nu,\mathrm{Jy\cdot ms}}$ is the fluence (in Jy·ms), $\Delta\nu_{\mathrm{GHz}}$ is the bandwidth (in GHz), $B_{0,15}$ is the surface magnetic field (normalized to 10^{15} G), $f_b = \delta\Omega/4\pi$, and z is the redshift of the source. The situation is more complicated for repeaters, where the constraint is on the total energy emitted by all bursts. Stringent efficiency constraints can be derived from FRB 121102. A 47 day observation of FRB 121102 with FAST reported 1652 bursts over 59.5 hr (Li et al. 2021), corresponding to an active phase duty cycle of $\zeta \approx 0.05$. The total source energy corresponding to these bursts is $E_{tot}\eta_r \simeq 6 \times 10^{42}\mathrm{erg} \times F_b(\zeta/0.05)^{-1}$ (Zhang 2022). Here $F_b = \Delta\Omega/4\pi$ is the global beaming factor, which encompasses the solid angle of all bursts and is in general much greater than f_b. The efficiency constraint from FRB 121102 is then

$$\eta_r \gtrsim 1.8 \times 10^{-5} \times F_b B_{0,15}^{-2}\left(\frac{\zeta}{0.05}\right)^{-1}. \tag{14}$$

The radio efficiency in our model, $\eta_r = \eta_{\gamma\to a} \times \eta_{a\to\gamma}$, can be computed from Equations (8) and (11). In Figure 2, we show the minimum axion–photon coupling ($g_{a\gamma\gamma}$) at a given mass (m_a) consistent with the efficiency constraints defined above. In this plot, we assume the Alfvén wave becomes charge starved at a distance of $10\,R_{ns}$ and adopts Alfvén wave parameters,

$\omega_A = 2\pi/\mathrm{km}$, $k_\perp = 0.1\omega_A$, $\varepsilon = 10^{-3}$, and $\gamma_0 = 10^4$. We also assume a beaming factor $f_b = 0.01$ for a single burst and $F_b = 0.1$ for the repeater. For reconversion in the wind, we assume the preflare wind luminosity is enhanced by a factor of 10^2 compared to that of the persistent wind and that the pair multiplicity factor is $\mathcal{M} = 10^2$.

6. Discussion and Conclusions

While inner magnetar magnetosphere models of FRBs successfully explain many observed temporal and polarimetric features, general arguments suggest that FRBs are susceptible to strong scattering as they propagate through the magnetosphere (Lyubarsky 2020; Beloborodov 2021), necessitating a viable transport model. Motivated by this, we propose that FRBs may be transported out of the magnetosphere due to their mixing with axions. Ultralight axions naturally mix strongly with electromagnetism only very close to the magnetar surface and far outside the light cylinder, where the plasma frequency in the wind coincides with the axion mass. Any inner-magnetosphere production of FRBs that is accompanied by large $E_\parallel$ necessarily produces axions in great abundance. As axions propagate through the magnetosphere, they effectively decouple from the plasma as the magnetic field drops. In the enhanced, preflare magnetar wind, axions encounter a plasma with monotonically decreasing plasma frequency and eventually reach a critical radius at which the axion mass coincides with the plasma mass. At this level crossing, axions mix strongly with radio photons, even in a weaker magnetic field.

We have presented a concrete model in which Alfvén waves, produced by a magnetar flare, become charge starved in the inner magnetosphere and produce O modes (Kumar & Bošnjak 2020) and axions through a two-stream instability though we reiterate that our mechanism is viable for any inner-magnetosphere emission mechanism that hosts large $E_\parallel$. The axions then resonantly reconvert to coherent radio waves in the wind. This model successfully explains many observational properties of FRBs. First, we have shown that in this mechanism, a large fraction of the flare magnetic energy can be converted to outgoing radio photons, satisfying FRB efficiency constraints. The axion burst produced in the inner magnetosphere has rapid temporal variability that is retained throughout its propagation, consistent with observations. Our scenario predicts a high degree of linear polarization, set by the magnetic field in the conversion region. Crucially, this class of models allows for FRBs to escape through both the open and closed magnetosphere, obviating the need for beamed emission along open field lines.

Finally, we comment that a smoking-gun signal of axion-mediated FRBs is the presence of axion counterparts associated with FRBs. We explore the prospects for observing these counterparts with dedicated axion detection experiments in upcoming work.

ORCID iDs

Anirudh Prabhu ⓘ https://orcid.org/0000-0001-9115-7844

References

Arvanitaki, A., Dimopoulos, S., Dubovsky, S., Kaloper, N., & March-Russell, J. 2010, PhRv, 81, 123530
Battye, R. A., Darling, J., McDonald, J., & Srinivasan, S. 2021a, PhRv, 105, L021305
Battye, R. A., Garbrecht, B., McDonald, J., & Srinivasan, S. 2021b, JHEP, 2021, 105
Battye, R. A., Garbrecht, B., McDonald, J. I., Pace, F., & Srinivasan, S. 2020, PhRvD, 102, 023504
Beloborodov, A. M. 2017, ApJL, 843, L26
Beloborodov, A. M. 2020, ApJ, 896, 142
Beloborodov, A. M. 2021, ApJL, 922, L7
Buckley, J. H., Dev, P. B., Ferrer, F., & Huang, F. P. 2021, PhRvD, 103, 043015
Burrows, A., Ressell, M. T., & Turner, M. S. 1990, PhRvD, 42, 3297
Caputo, A., Raffelt, G., & Vitagliano, E. 2022, PhRvD, 105, 035022
CAST 2017, NatPh, 13, 584
Dessert, C., Dunsky, D., & Safdi, B. R. 2022, PhRvD, 10, 103034
Dessert, C., Foster, J. W., & Safdi, B. R. 2020, PhRvL, 125, 261102
Dessert, C., Long, A. J., & Safdi, B. R. 2019, PhRvL, 123, 061104
Dine, M., & Fischler, W. 1983, PhLB, 120, 137
Fortin, J.-F., Guo, H.-K., Harris, S. P., Sheridan, E., & Sinha, K. 2021, JCAP, 2021, 036
Fortin, J.-F., & Sinha, K. 2018, JHEP, 2018, 48
Fortin, J.-F., & Sinha, K. 2019, JHEP, 2019, 163
Foster, J. W., Witte, S. J., Lawson, M., et al. 2022, PhRvL, 129, 251102
Foster, Joshua W., Kahn, Yonatan, Macias, Oscar, et al. 2020, PhRvL, 125, 171301
Hoof, S., & Schulz, L. 2022, arXiv:2212.09764
Hook, A., Kahn, Y., Safdi, B. R., & Sun, Z. 2018, PhRvL, 121, 241102
Huang, F. P., Kadota, K., Sekiguchi, T., & Tashiro, H. 2018, PhRvD, 97, 123001
Iwazaki, A. 2015, PhRvD, 91, 023008
Katz, J. I. 2017, MNRAS: Letters, 471, L92
Katz, J. I. 2020, MNRAS: Letters, 494, L64
Katz, J. I. 2022, MNRAS: Letters, 516, L58
Keil, W., Janka, H.-T., Schramm, D. N., et al. 1997, PhRvD, 56, 2419
Kennel, C. F., & Coroniti, F. V. 1984, ApJ, 283, 694
Kumar, P., & Bošnjak, Ž. 2020, MNRAS, 494, 2385
Kumar, P., Gill, R., & Lu, W. 2022, MNRAS, 516, 2697
Kumar, P., Lu, W., & Bhattacharya, M. 2017, MNRAS, 468, 2726
Leroy, M., Chianese, M., Edwards, T. D. P., & Weniger, C. 2020, PhRvD, 101, 123003
Li, D., Wang, P., Zhu, W. W., et al. 2021, Natur, 598, 267

Li, J., Spitkovsky, A., & Tchekhovskoy, A. 2012, ApJ, 746, 60
Li, L.-B., Huang, Y.-F., Geng, J.-J., & Li, B. 2018, RAA, 18, 061
Li, X., & Beloborodov, A. M. 2015, ApJ, 815, 25
Lu, W., Kumar, P., & Zhang, B. 2020, MNRAS, 498, 1397
Luo, R., Wang, B. J., Men, Y. P., et al. 2020, Natur, 586, 693
Lyubarsky, Y. 2020, ApJ, 897, 1
Mahlmann, J. F., Philippov, A. A., Levinson, A., Spitkovsky, A., & Hakobyan, H. 2022, ApJL, 932, L20
Marsh, M. D., Russell, H. R., Fabian, A. C., et al. 2017, JCAP, 2017, 036
Mehta, V. M., Demirtas, M., Long, C., et al. 2021, JCAP, 2021, 033
Metzger, B. D., Margalit, B., & Sironi, L. 2019, MNRAS, 485, 4091
Millar, A. J., Baum, S., Lawson, M., & Marsh, M. D. 2021, JCAP, 2021, 013
Nimmo, K., Hessels, J. W. T., Kirsten, F., et al. 2022, NatAs, 6, 393
Noordhuis, D., Prabhu, A., Witte, S. J., et al. 2022, arXiv:2209.09917
Peccei, R. D., & Quinn, H. R. 1977a, PhRvL, 38, 1440
Peccei, R. D., & Quinn, H. R. 1977b, PhRvD, 16, 1791
Philippov, A., Timokhin, A., & Spitkovsky, A. 2020, PhRvL, 124, 245101
Philippov, A., Uzdensky, D. A., Spitkovsky, A., & Cerutti, B. 2019, ApJ, 876, L6
Porth, O., Komissarov, S. S., & Keppens, R. 2014, MNRAS, 443, 547
Prabhu, A. 2021, PhRvD, 104, 055038
Prabhu, A., & Rapidis, N. M. 2020, JCAP, 10, 054
Preskill, J., Wise, M. B., & Wilczek, F. 1983, PhLB, 120, 127
Pshirkov, M. S. 2017, IJMPD, 26, 1750068
Pshirkov, M. S., & Popov, S. B. 2009, JETP, 108, 384
Raffelt, G., & Stodolsky, L. 1988, PhRvD, 37, 1237
Reynolds, C. S., Marsh, M. C. D., Russell, H. R., et al. 2020, ApJ, 890, 59
Ruderman, M. A., & Sutherland, P. G. 1975, ApJ, 196, 51
Safdi, B. R., Sun, Z., & Chen, A. Y. 2019, PhRvD, 99, 123021
Schindler, K., Hesse, M., & Birn, J. 1988, JGRA, 93, 5547
Sikivie, P. 1983, PhRvL, 51, 1415
Sisk-Reynés, J., Matthews, J. H., Reynolds, C. S., et al. 2021, MNRAS, 510, 1264
Slane, P. 2017, Handbook of Supernovae (Cham: Springer), 2159
Sridhar, N., Metzger, B. D., Beniamini, P., et al. 2021, ApJ, 917, 13
Svrcek, P., & Witten, E. 2006, JHEP, 2006, 051
Thornton, D., Stappers, B., Bailes, M., et al. 2013, Sci, 341, 53
Tkachev, I. I. 2015, 101, 1
Wadiasingh, Z., Beniamini, P., Timokhin, A., et al. 2020, ApJ, 891, 82
Wadiasingh, Z., & Timokhin, A. 2019, ApJ, 879, 4
Weinberg, S. 1978, PhRvL, 40, 223
Wilczek, F. 1978, PhRvL, 40, 279
Witte, S. J., Noordhuis, D., Edwards, T. D., & Weniger, C. 2021, PhRvD, 104, 103030
Wouters, D., & Brun, P. 2013, ApJ, 772, 44
Yuan, Y., Beloborodov, A. M., Chen, A. Y., & Levin, Y. 2020, ApJ, 900, L21
Zhang, B. 2018, ApJL, 867, L21
Zhang, B. 2022, arXiv:2212.03972